Journal of Hydrology: Regional Studies 30 (2020) 100704

Contents lists available at ScienceDirect

Journal of Hydrology: Regional Studies

journal homepage: www.elsevier.com/locate/ejrh

Catchment-scale flood hazard mapping and flood vulnerability analysis of residential buildings: The case of Khando River in eastern Nepal

Saraswati Thapa[a], Anup Shrestha[a], Suraj Lamichhane[a], Rabindra Adhikari[b,c], Dipendra Gautam[b,c,d,e,*]

[a] Department of Civil Engineering, Institute of Engineering, Pulchowk Campus, Lalitpur, Nepal
[b] Department of Civil Engineering, Cosmos College of Management and Technology, Lalitpur, Nepal
[c] Structure and Infrastructure Dynamics Laboratory (SID-Lab), Interdisciplinary Research Institute for Sustainability, IRIS, Kathmandu, Nepal
[d] Department of Civil Engineering, Institute of Engineering, Thapathali Campus, Kathmandu, Nepal
[e] Associate Fellow, Nepal Academy of Science and Technology, Lalitpur, Nepal

ARTICLE INFO

Keywords:
Flood hazard mapping
Flood vulnerability
Flood fragility function
Khando River
Residential building

ABSTRACT

Study region: This study considers the Khando River (a tributary of Koshi River) in eastern Nepal.
Study focus: To quantify the hazard and vulnerabilities across one of the frequently flooding catchments, i.e. Khando River, we conducted flood hazard assessment for 20, 50, 100, and 200 years return periods. We coupled flood hazard analysis with vulnerability analysis of the most dominant construction system along the river channel, i.e. wattle and daub houses. Based on the measured inundation depths, we created vulnerability and fragility functions. The flood hazard maps, damage mechanisms due to the 2017 flood, and vulnerability, as well as fragility, curves are reported in this paper.
New Hydrological Insights for the Region: The flood hazard analysis highlighted that the 2017 flood was equivalent to 20 years return period flood. Flood hazard analysis shows that the variation in the maximum inundation depth is not so wide between 20 and 200 years return periods for the Khando River catchment. Flood vulnerability analysis of residential houses along the riverbank highlighted that the wattle and daub construction system is highly vulnerable even for 20 years return period flood. Thus, the floods equivalent to 50, 100, and 200 years may have detrimental consequences in the future.

1. Introduction

Flood, overflow of water beyond the river channel, is one of the major natural hazards that causes enormous loss of lives and properties worldwide every year. Floods become more severe once they pass through built-up areas and arable lands as in the case of 1993 flood in Nepal, 2008 Koshi flood in eastern Nepal (Government of Nepal, 2009), and the 2017 central Nepal water flood (Gautam and Dong, 2018). Several historical flood events show that the major losses are incurred across the river and rivulet channels. For instance, the 1993 floods across Nepal, 2002 central Nepal flood, 2008 Koshi river flood, 2008 Western Nepal flood, 2012 Seti river flood, 2017 flood across Nepal, among others reflected that the major losses had occurred along the riverbanks. The

* Corresponding author at: Department of Civil Engineering, Cosmos College of Management and Technology, Lalitpur, Nepal.
E-mail addresses: saraswati.thapa@pcampus.edu.np (S. Thapa), anup.shrestha@sagarmatha.edu.np (A. Shrestha), surajlamichhane@ioe.edu.np (S. Lamichhane), rabindraadhi@cosmoscollege.edu.np (R. Adhikari), dipendra01@tcioe.edu.np (D. Gautam).

https://doi.org/10.1016/j.ejrh.2020.100704
Received 23 March 2020; Received in revised form 9 June 2020; Accepted 9 June 2020
Available online 17 June 2020

1993 flood in Nepal caused 1170 fatalities and damaged some 32,765 buildings (Government of Nepal, 2009). Similarly, the 2008 Koshi flood displaced around 65,000 people in Saptari and Sunsari in eastern Nepal (Government of Nepal, 2009). The 2017 flood in Nepal destroyed 41,625 and damaged 150,510 houses leading to an overall loss of US$ 187.9 million (Government of Nepal, 2017). The post-flood recovery needs assessment conducted after the 2017 flood events in Nepal depicted that 53.3 % of total recovery needs was required for housing sector only (Government of Nepal, 2017). The Department of Hydrology and Meteorology (DHM) recorded the highest ever mean rainfall of 1800 mm, substantially exceeding the average of 1200 mm in 2017 (Government of Nepal, 2017). A total of 7141 families were affected along with the total economic loss of US$ 7.8 million during 2015 and 2016 floods in Nepal (Government of Nepal, 2020). Most of the flood events worldwide have depicted that the impacts of floods on built environment would be disastrous (see e.g. (Government of Nepal, 2009; Guzzetti et al., 2005; Marchi et al., 2010; Cao et al., 2016; Santo et al., 2016; Tsakiris, 2014; Fuchs et al., 2007; Santos et al., 2015; Gautam and Dong, 2018), among others). As losses are inevitable due to floods, many researchers have considered flood hazard mapping as one of the most efficient tools for prevention to mitigation. In recent decades, many researchers have performed flood hazard mapping in various parts of the world as reported elsewhere (see e.g. (Hagen et al., 2010; Di Salvo et al., 2018; Nharo et al., 2019; Popa et al., 2019; Zhang et al., 2015; Ntajal et al., 2017); among others). For flood modeling, HEC-RAS (Hydrologic Engineering Center-River Analysis System) (US Army Corps of Engineers, 2020), HEC-geoRAS (Hydrologic Engineering Center-Geospatial River Analysis System) (ESRI, 2020), and GIS (Geographical Information System) (ESRI, 2020) are extensively used by researchers (see e.g. (Sarhadi et al., 2012), (Ben Khalfallah and Saidi, 2018; Ezz, 2018; Miranda and Ferreira, 2019; Santo et al., 2016), among others). Generally, basin-scale flood hazard mapping is performed worldwide (e.g. (Grimaldi et al., 2013; Bourenane et al., 2019; Zhao et al., 2019; Shadmehri Toosi et al., 2019; Kazakis et al., 2015), among others); however, limited works exist in literature for Nepali river basins (e.g. (Mishra and Herath, 2015; Khanal et al., 2007)).

Flood damage to structures and lifelines and losses to lives and property prompt crucial planning in terms of flood hazard mapping and mitigation strategies. The problem of floods in many urban and rural areas of Nepal is still severe as floods would generally affect Nepal in almost every monsoon. Most of the flood victims would be the people living in the flood plain areas as in the case of 2008 Koshi flood and 2017 central Nepal flood. Although flood damage is widespread, and losses are enormous, due attention is yet to be paid in terms of hazard, vulnerability, and risk studies across Nepal. Gautam (2017a,b) presented a generic flood risk map for the southern part of Nepal; however, the map is based on topographical features only so it may not be exhaustive to represent the flood scenarios. This necessitates basin-scale studies to assess the flood hazard which may be helpful in designing countermeasures and preparedness initiatives to downscale the losses. The annual torrential precipitation (Talchabhadel et al., 2018), high surface run-off rate, deforestation, urban expansion, and land-use change (Lamichhane and Shakya, 2019a,b) could lead to frequent flooding events. As the land use/cover change dynamics seems rapidly changing even within a short time (Lamichhane and Shakya, 2019a,b), there is also a high risk of frequent and devastating flood events in Nepal.

The flood events can neither be controlled completely nor the effects could be completely checked; however, the flood impacts can be minimized by structural and non-structural mitigation measures. For effective planning and understanding, flood vulnerability analysis of structures and infrastructures is one of the rational approaches. Flood vulnerability analysis of the built environment is gaining attention in recent decades and many researchers are paying attention to develop flood vulnerability functions (see e.g. (Fuchs et al., 2019a,b; Baradaranshoraka et al., 2019; De Risi et al., 2019), among others). The vulnerability, as well as fragility, functions depict the probability of occurrence of particular damage under the flood intensity level. Fragility and vulnerability functions are important tool for estimating flood effects prior to the flood as well as to prioritize response and recovery efforts after flood events considering the built environment. To the best of authors' knowledge, vulnerability and fragility functions for buildings in Nepal do not exist. It is worthy to note that Gautam and Dong (2018) constructed depth-damage curves for residential stone masonry buildings using the damage data after the 2017 flood. Similarly, Adhikari et al. (2019) constructed flood and multi-hazard fragility functions for highway bridges in Nepal using a heuristic approach. After the 2017 floods in eastern and central Nepal, flood damage to the structures and infrastructures and associated losses are more pronounced as frequent floods are inevitable in Nepal.

In this paper, we perform flood hazard mapping for Khando River catchment in eastern Nepal which observes frequent floods and attributed damages and losses are severe. Together with flood hazard maps for various intervals, we present flood vulnerability analysis of wattle and daub dwellings which is the most dominant construction system across the riverbanks. Most of the historical flood damage reports show that the worst affected building type would be the wattle and daub construction (NPC, 2017). Thus, we present the vulnerability and fragility functions for residential wattle and daub dwellings together with flood hazard maps for 20, 50, 100, and 200 years return periods in this study.

2. Material and methods

2.1. Study area

Nepal is situated between longitude 80° 4′ E to 88° 12′E and latitude 26° 12′ N to 30° 27′ N. The elevation of the country varies from 60 m at Jhapa in the south to 8848 m at the Mt. Everest in the north within a short horizontal distance of 90–120 km. The spatio-temporal variation of precipitation is very high due to the variation in topography (Talchabhadel et al., 2018; Karki et al., 2017). The precipitation variation ranges from less than 300 mm in dry rain shadow regions to more than 5000 mm in wet region in Lumle of Kaski district in western Nepal (Department of Hydrology and Meteorology, 2020). About 6000 rivers and rivulets are in Nepal with a total length exceeding 45,000 km and with the total drainage area of 191,000 sq. km. Khando River is a non-perennial spring river that mainly passes through Saptari district in eastern Nepal and meets the Koshi River (Fig. 1). Saptari district covers an area of 1363 km^2 and has a population of 639,284 per the 2011 census (Central Bureau of Statistics Nepal, 2012). The total building population in

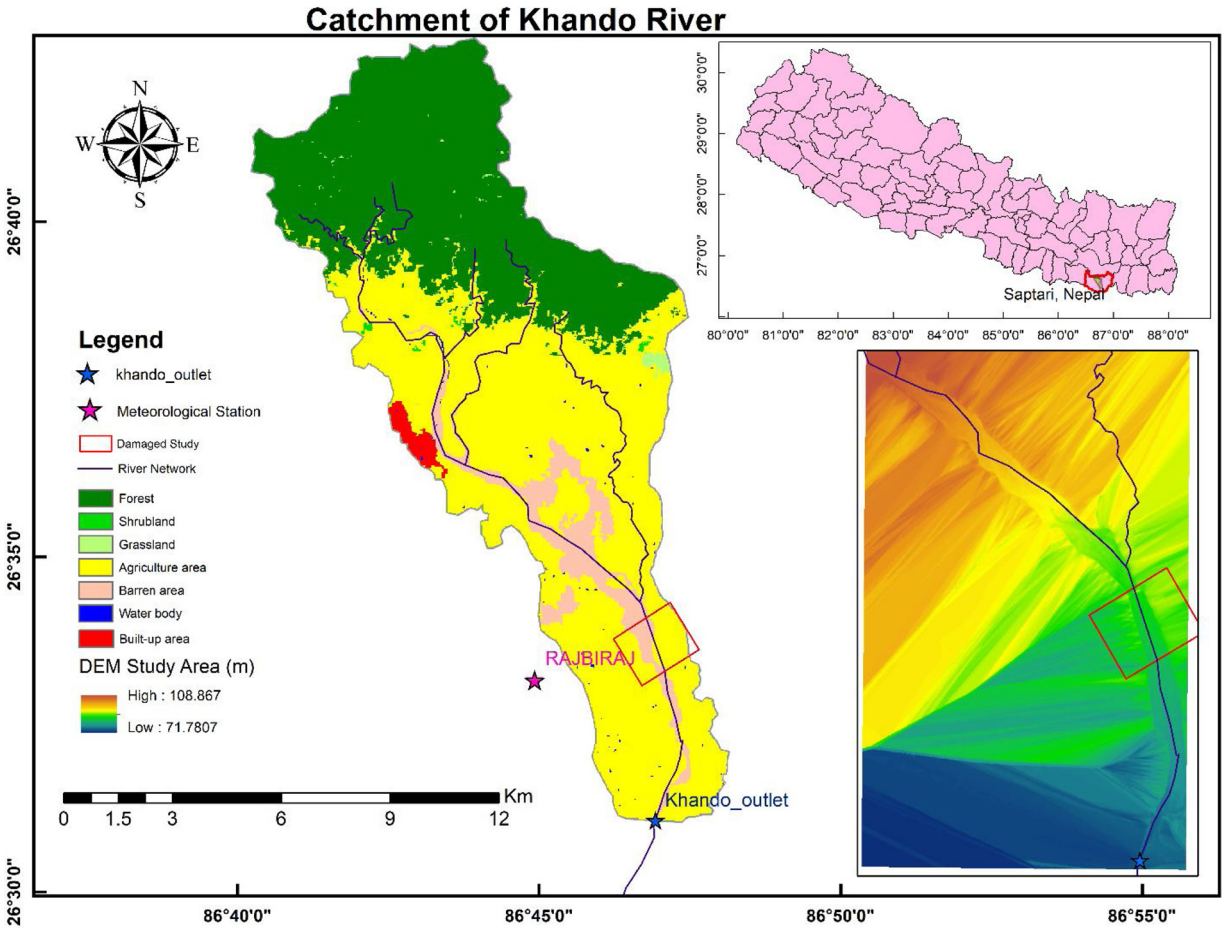

Fig. 1. The Khando River catchment in eastern Nepal.

Saptari district was 121,064 in 2011, among them 62,465 buildings were wattle and daub houses (Central Bureau of Statistics Nepal, 2012). The catchment area of the Khando River is 117.3 km^2 and elevation ranges between 67–419 m from the average mean sea level. Per the long-term climate data (1986–2015) recorded in the catchment, the annual average rainfall is ~1800 mm (Talchabhadel et al., 2018). Similarly, annual maximum and minimum temperatures in the catchment are ~33.7 °C in May and ~8 °C in January based on the long-term climate data (1981–2012) (Department of Hydrology and Meteorology, 2020). The length of the river is 25.246 km. Khando River is one of the most notorious rivers in terms of flooding and associated damages as per the records of floods in recent decades (see e.g. (NPC, 2017; Government of Nepal, 2009)). The majority of the river stretch lies in the Indo-Gangetic plain, so the river is flat with an average bank height of ~0.8 m. Moreover, the river would be dry for most of the period except for the rainy season. The river has a meandering channel; however, we did not observe significant channel shifting between 2015 and 2017. We have considered the width of the study area from 800 to 1000 m. Geologically, Khando River catchment is characterized by loose pebbles and cobbles. Being a river originated from the Siwalik region, Khando River has also high sediment transport rate and the aggradation of the river channel is quite common. The catchment has drainage density of 0.47 km/km^2, average permeability of 25 − 75 m/day, and the time of concentration of the catchment is 4.129 h based on the Kirpich equation (Maidment, 1992). After the Siwalik region, the flood plain area of the Khando River increases due to significant reduction in river slope. As shown in Fig.1, the largest fraction of land use is associated with agriculture. The northern part of the catchment mainly comprises the forest and shrubland. However, the southern part of the catchment comprises agricultural and barren areas. The barren areas would be generally comprised by slums and squatter settlements. As the entire catchment is not densely populated, the land use map does not clearly depict the built-up areas due to scattered settlements. The northern part of the catchment is less populated than the southern part. The southern part of the catchment comprises densely populated settlements even in the riverbanks. As the settlements beside the riverbanks are usually slums and squatter settlements, housing typology predominates the wattle and daub constructions with some brick masonry buildings. Every year thousands of people become homeless due to the flooding in the Khando River and losses would be attributed to crops, livestock, and infrastructure damage as well.

2.2. Methodology

2.2.1. Flood hazard mapping

To assess the flood hazard across the Khando River catchment, we collected the topographical survey data and prepared digital elevation model (DEM) for both left and right banks of Khando River using Kriging's interpolation tool as it is a fast and flexible method of creating DEMs (Pavlova, 2017). Furthermore, we prepared 12.5×12.5 m resolution DEM in Arc GIS by creating Triangular Irregular Network (TIN) from topographic survey data. The topographic survey was conducted in 2015 using Total Station having the least count of 0.001 m for 30 km longitudinal chainage and ~1000 m cross-section that includes upstream and downstream of the damage location. The accuracy of the created DEM was confirmed with the freely available open street map in Arc GIS. We collected SRTM (Shuttle Radar Topography Mission) 30 m (SRTM Digital Elevation Database, 2020) DEM and performed spatial analysis to depict the flow direction, flow accumulation, and watershed delineation. Both DEM and spatial analysis were performed in Arc GIS 10.3.1 environment. The processed raster was then subject to HEC-geoRAS preprocessing. We digitized and formulated TINs for channels, riverbanks, flow path lines, and cross-section cutline. Rainfall data from a nearby meteorological station (see Fig. 1) was collected from the Department of Hydrology and Meteorology, Government of Nepal. Rainfall data between 1972–2018 was employed for the analysis. The daily rainfall range was between 42–245.5 mm/day for the recorded period. The annual wetness index for the catchment is 1600 mm (Talchabhadel et al., 2018). We trialed several methods to estimate the flood discharge and adopted Hydest2004 DHM approach (Department of Hydrology and Meteorology, 2020) as it was exclusively derived and implemented for un-gauged rivers in Nepal. Hydest2004 DHM method is the modification of the WECS 1990 (Water and Energy Commission Secretariat) method (Department of Hydrology and Meteorology, 2020). Hydest2004 DHM method treats the entire country as a single hydrological region and performs regionalization for low flows, long term flows, and flood flows. This method estimates discharges for 2 and 100 years return periods first and facilitates the discharge estimation for any other return period based on empirical formulas (for further details, see: https://www.dhm.gov.np/). Furthermore, a comparison between several other approaches highlighted that Hydest2004 DHM approach results in the highest discharge. The outputs of HEC-geoRAS preprocessing provided GIS to RAS import files, thereafter, one-dimensional hydrodynamic models were created in HECRAS 5.0.7 for the flood frequency analysis of 20, 50, 100, and 200 years return periods. Firstly, we analyzed observed rainfall data from the nearby meteorological station (see Fig. 1) and found the daily maximum rainfall for the day on which flood event occurred (August 13, 2017). The recorded maximum daily rainfall was 207.5 mm, which nearly coincides with 20 years return period. Thus, we opted 20 years as one return interval together 50, 100, and 200 as scenario return intervals for severer floods than that of 2017. The Manning's 'n' value, flow data, and boundary conditions were inputted in the imported GIS2RAS file and the HECRAS results were obtained. To perform HECRAS analysis, we inputted critical depth as the boundary condition and mixed flow regime. The flow data obtained from Hydest 2004 DHM method and geometry obtained from the DEM created from survey data were also inputted. The cross-sections were created in HEC-geoRAS at 200 m intervals for 1000 m width. We adopted Manning's roughness coefficient 0.035 for the river channel and 0.04 for the banks (Gautam and Dulal, 2013) as Khando River is a tributary of Koshi River Basin. Thereafter, we obtained the water surface profiles and checked the sufficiency of cross-section coverage. If the decision led to insufficient cross-sections, HEC-geoRAS preprocessing was repeated as shown in Fig. 2. In the case of enough cross-section coverage, the outputs were exported to GIS from HECRAS and water surface TINs were created in Arc GIS environment. Thereafter, flood plain extent and depth grids were obtained and flood hazard maps for 20, 50, 100, and 200 years return period were prepared using Arc GIS. The step-by-step procedures to obtain the flood hazard maps are shown in detail in Fig. 2.

2.2.2. Flood vulnerability of residential building

To obtain flood vulnerability functions, most of the researchers have used inundation depth as the intensity measure (see e.g. (Fuchs et al., 2019a,b; Godfrey et al., 2015; Karagiorgos et al., 2016), among others). We also used inundation depth to derive fragility and vulnerability functions using the depth and damage data collected after the 2017 flood in eastern Nepal. We measured the depth of inundation and estimated the damage extent (damage ratio) for wattle and daub dwellings, brick masonry, reinforced concrete (RC) constructions in the affected areas of Saptari district. As masonry and RC building damage were limited, the most extensively damaged construction system, i.e. wattle and daub, is incorporated in this study to delineate flood vulnerability to residential buildings. The damage ratio was estimated as the fraction of total repair cost to the overall cost of new construction. As the direct evaluation of the damage extent would be affected by biases such as erroneous and subjective judgments, we first estimated the overall cost of construction interviewing the local people and flood victims and then assessed the damage to individual houses to obtain the damage ratio. The damage ratio was assigned between 0–1. The damage ratio value 1 indicates the complete collapse of a building (new construction required), whereas, the 0 value of damage ratio indicates the building remained unharmed due to the flood. The depth of inundation was measured directly in-situ by measuring tapes. Logit function was chosen to construct the vulnerability (depth-damage) function fitting the depth and damage data. It is worthy to note that several researchers have considered various statistical distributions to construct vulnerability/fragility functions (see e.g. (Shinozuka et al., 2002; Porter et al., 2007; Rossetto and Elnashai, 2005; Gautam et al., 2018; Gautam, 2017a,b; Parisi and Sabella, 2017)). Among them, Weibull, modified Weibull, linear, second-order polynomial, logistic function, third order polynomial, among others are commonly practiced (for further details, see: (Fuchs et al., 2007; Totschnig and Fuchs, 2013), among others). Based on the collected information, fragility functions for discrete damage classes were also constructed using lognormal distribution. In total, we assessed 34 damaged wattle and daub houses and processed the data to construct vulnerability function and fragility functions. Most of the wattle and daub buildings would be swept away by the water current so it is very difficult to find many cases of damage across the main river channel. As post-flood damage data are rare, most of the researchers previously derived vulnerability/fragility functions using limited data sets. For

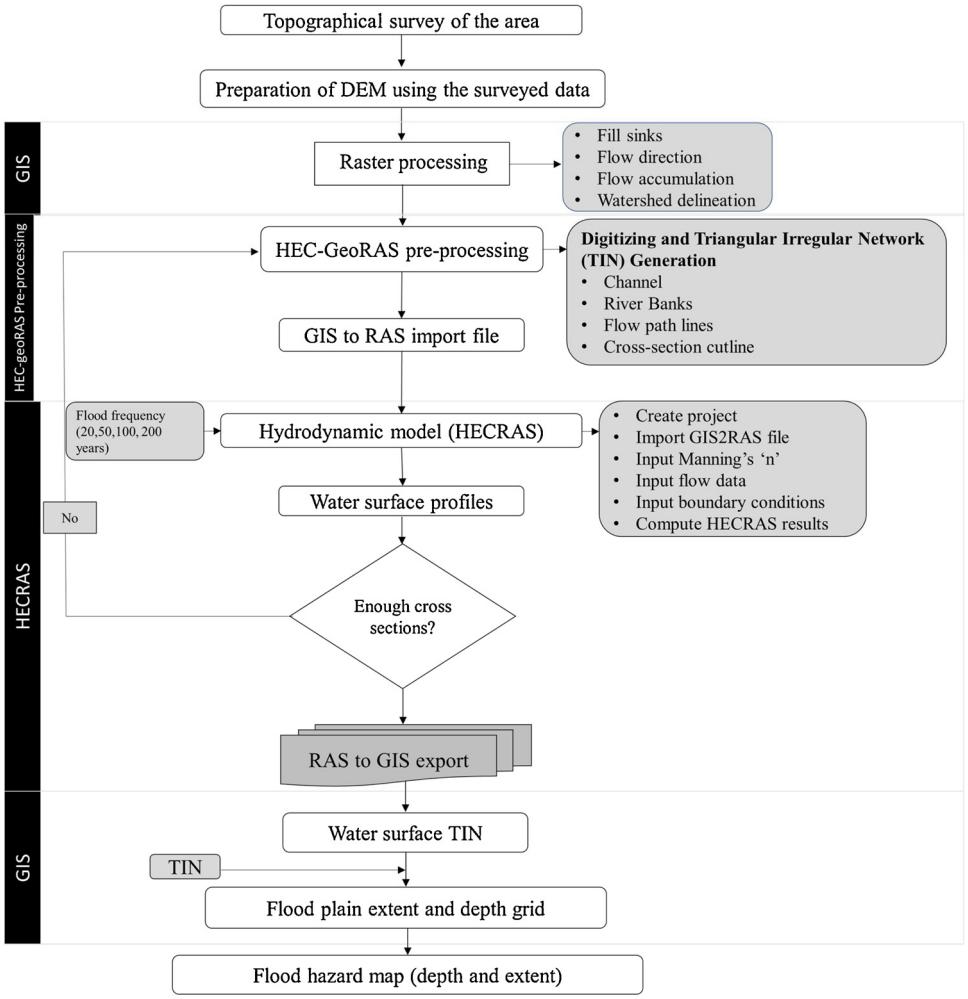

Fig. 2. Flood hazard mapping framework.

example, (Godfrey et al., 2015) used 24, Quan Luna et al. (2011) used 13, Totsching et al. (Totschnig and Fuchs, 2013) used 67, Azmeri and Isa (2018) used 38, Kang and Kim (2016) used 25, and Papathoma-Kohle et al. (Papathoma-Köhle et al., 2012) used 51 building damage data to construct vulnerability function. As real flood damage data are valuable because of their exact representation, the vulnerability/fragility functions constructed using the real damage data would be more representative than the simulated ones. Thus, many researchers are developing vulnerability functions even with limited datasets. Furthermore, in the case of the availability of discrete damage data, it would be imperative to construct fragility functions so that the probability of exceedance of various damage states would be discretely presented. It is because the damageability function reflects just the damage or non-damage scenario in a particular inundation depth. To date, most of the researchers have used lognormal distribution for the post-disaster database (e.g. (Porter et al., 2007; Gautam et al., 2018; Shinozuka et al., 2002); among others). We also fitted two-parameter lognormal fragility functions for five damage classes: minor, major, severe, beyond repair, and collapse. The damage classes were determined based on the mean damage ratio that was assigned to each surveyed building. The minor, major, severe, beyond repair, and collapse damage states correspond to damage ratios of 0.15, 0.35, 0.50, 0.80, and 1 respectively. For each intensity measure (IM) level, the probability of reaching or exceeding the particular damage state (DS), can be presented as a two-parameter lognormal distribution function F(x) using the maximum likelihood approach. The likelihood function for lognormal fragility can be expressed as:

$$L = \prod_{i=1}^{N} [F(x_i)]^{y_i} [1 - F(x_i)]^{1-y_i} \ldots \quad (1)$$

Where $F(\cdot)$ is the fragility function for the specific damage state; a_i is the measured depth of inundation (m) for the affected building i; y_i is 1 or 0 based on the damage status of the buildings exposed to a_i ; and N is the total number of buildings. The two-parameter fragility function, F(x), can be represented as:

$$F(x) = \Phi\left[\frac{\ln(x) - \ln(\alpha)}{\beta}\right] ...(2)$$

where $\Phi[\cdot]$ represents standardized normal distribution function; and α and β are the median and dispersion parameters of the lognormal distribution. The parameters α and β are estimated satisfying the following conditions:

$$\frac{d\ln(L)}{d\alpha} = \frac{d\ln(L)}{d\beta} = 0 ... \quad (3)$$

3. Results and discussions

We conducted flood hazard analysis and flood vulnerability analysis of wattle and daub houses which is a dominant construction system along the Khando Riverbank in eastern Nepal. The results are reported in terms of flood hazard maps, flood performance of residential buildings, and flood vulnerability of wattle and daub buildings separately in the following sections.

3.1. Flood hazard mapping

First, we obtained discharges for 20, 50, 100, and 200 years return periods. The instantaneous flood discharges were obtained as 408, 534, 660, and 754 m^3/s for 20, 50, 100, and 200 years return periods. Fig. 3a shows that the maximum inundation depth for 200 years return period is 4.2 m. Most of the areas across the catchment depict the inundation depth between 0.5–2.5 m for 200 years return period. Fig. 3a, b, c, and d highlight that the inundation depth was less in the left bank of the river due to higher topographical relief than the right bank.

As shown in Fig. 3b, the maximum inundation depth is 4.12 m for 100 years return period. The maximum inundation depths for 50 and 20 years return periods were obtained as 4 and 3.85 m respectively. The variation in the maximum inundation depth is not wide possibly because there is no significant elevation difference between the river channel and adjoining areas. Channel shifting and formation of artificial levees due to aggradation would act as the border between the river and agricultural land. This peculiarity sometimes leads to high inundation depth even beyond the river channel. Channel shifting in the Khando River occurs primarily due to the occurrence of loose soil and subsequent erosion. Fig. 3a, b, c, and d collectively delineate that with the decrement in inundation depth, the larger fraction of the catchment would be less inundated. This means when the maximum depth of inundation decreases, more areas tend to be exposed to less than 0.5 m inundation.

3.2. Flood vulnerability of residential wattle and daub buildings

3.2.1. Flood performance of residential buildings

After the 2017 flood in central and eastern Nepal, we conducted field surveys in the affected areas; mainly in Sunsari and Saptari districts in eastern Nepal. The survey was dedicated to assessing the damage mechanisms and damage levels in affected structures and infrastructures. The major damage location was across the Khando River in Saptari district. The most affected building form was the wattle and daub system. Similar observations were made also in Sunsari district. Wattle and daub constructions are low-cost folded bamboo constructions with thatched or galvanized iron (GI) roofing with bamboo or concrete post with marginal (usually single) reinforcement that would be available in the local market. Wattle and daub buildings are usually one to two-storied constructions that usually do not have specific foundations. Rather, bamboo or concrete pillars inserted on the ground serve as the foundation system. The pillars would not be tied at the plinth level; however, they would be tied at the eaves level with folded bamboo sheets. The wall system comprises the folded bamboo sheets or shrub shoots. The wall skeleton would be then plastered with the clay usually mixed with cow dung. The wall thickness would be uniform throughout the dwelling including the partition walls. As shown in Fig. 4a, the concrete pillars of a wattle and daub house were washed away by the flood. Due to the lack of adequate stiffness of walls and pillars, water current easily washed away the walls and pillars. We did not observe any connection to tie-up the structural system (pillars and walls), thus the effect of water current became more localized leading to the collapse of some parts of the house. Fig. 4b shows a washed away wattle and daub house that was fixed again for temporary use. It is worthy to note that the brittle damages in structural members were scarce; however, the poor connections and less depth of insertions on the ground fundamentally affected the performance of houses during flood. Fig. 4c shows the remains of a wall of wattle and daub house made up of bamboo pillars. As shown in Fig. 4c, a thin sheet of walls could be observed which leads to negligible stiffness against the water current during flooding. Fig. 4d displays a house with ejected and distorted concrete pillars together with some washed away wattle and daub walls. We measured the depth of inundation between $2-170$ cm in the affected areas. The inundation depth of 2 cm had negligible to slight damage in houses; however, 170 cm depth of inundation led to complete collapse to beyond repair damage level.

Nearby the East-West Highway in Saptari district, we observed a spectacular example of reinforced concrete (RC) building damage (Fig. 5a). At the depth of inundation of 2.5 m, the foundation of the building was washed away, and the frame was also heavily damaged. The building was under construction and we observed that the building was not code-conforming due to lack of adequate ductile detailing. The flooded water discharge got high velocity in a narrow channel passing through the foundation and heavy erosion occurred subsequently leading to the collapse the RC building. Fig. 5b shows an example of a concrete pillar inserted into the piled-up clay that serves as the plinth. It is obvious that once eroded, the pillars would distort or get washed away. In Fig. 5c, a mixed construction system could be observed that came into practice after the 2008 flood in the affected areas of Saptari and Sunsari

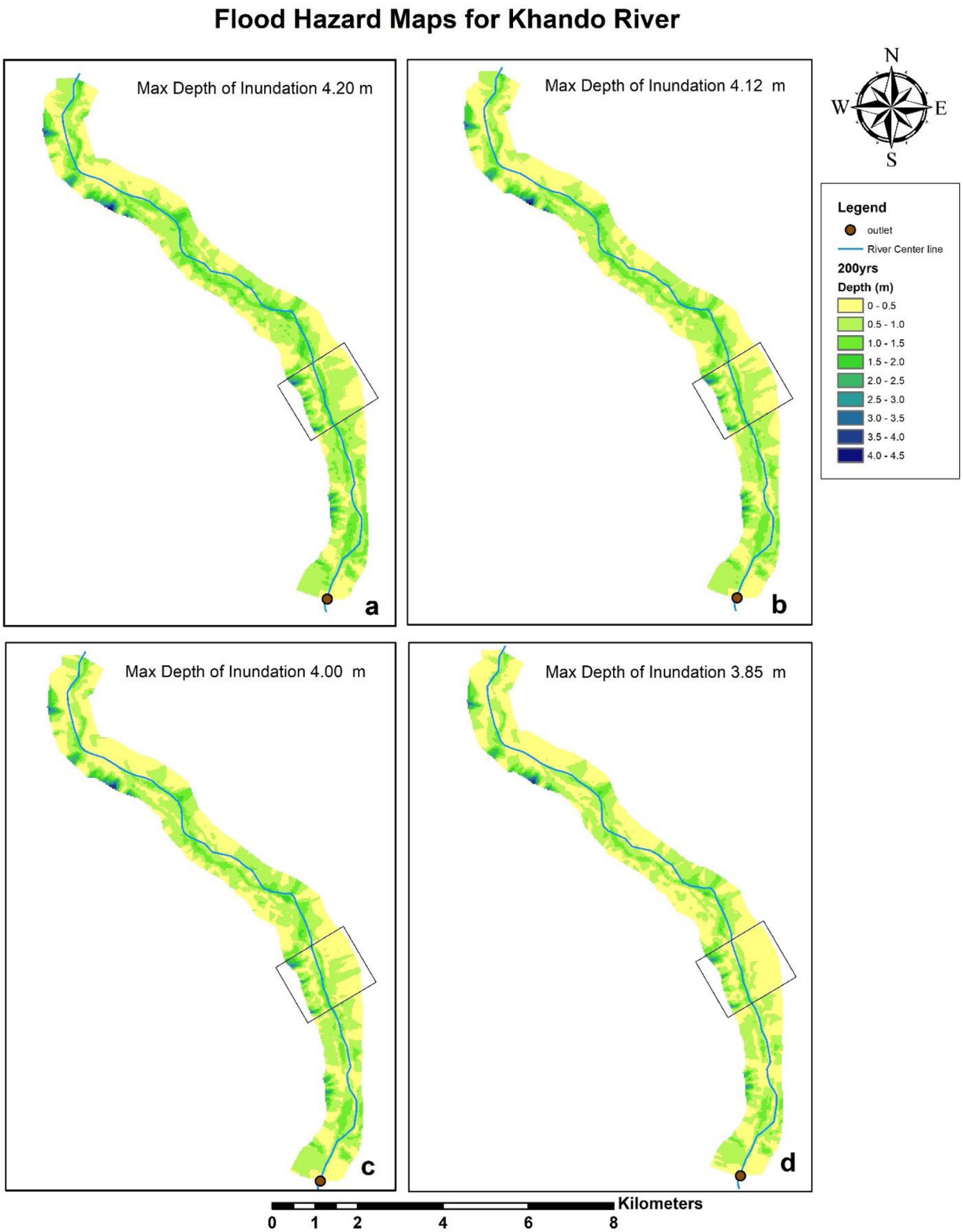

Fig. 3. a) Inundation map for 200 years return period, b) inundation map for 100 years return period, c) inundation map for 50 years return period, and d) inundation map for 20 years return period.

Fig. 4. a) Wattle and daub house partly damaged by flood, b) a destroyed wattle and daub house restored for temporary use, c) remains of a building (one wall) as three other walls were destroyed by the flood, d) a distorted wattle and daub house with collapsed and washed away walls.

Fig. 5. a) A washed away under-construction reinforced concrete building, b) ejected concrete pole displays the marginal depth of insertion to the ground, c) single wythed brick wall construction in the direction perpendicular to likely flood direction, d) vernacular multi-wythed flood resilient construction practice in southern Nepal.

districts. The walls normal to the likely flood direction were made up of single wythed brick masonry to increase stiffness; however, the orthogonal walls were still constructed using wattle and daub system. It is interesting to note that the first story of the house is constructed with brick and the second story was continued with wattle and daub system; possibly due to the assumption that the flood may rise to the first story level only. Such construction systems are designated to be flood resilient. Similar resilient practices are also reported elsewhere (see e.g. (Gautam et al., 2016)). Fig. 5d shows a vernacular form of a residential building in which the first story is a multi-wythed brick masonry and the second story comprises timber construction. The construction system in southern Nepal is mostly governed by reinforced concrete, brick masonry, and wattle and daub, notably, the importance of wattle and daub is more than any other building form due to several reasons. The first is that the wattle and daub construction is the most popular

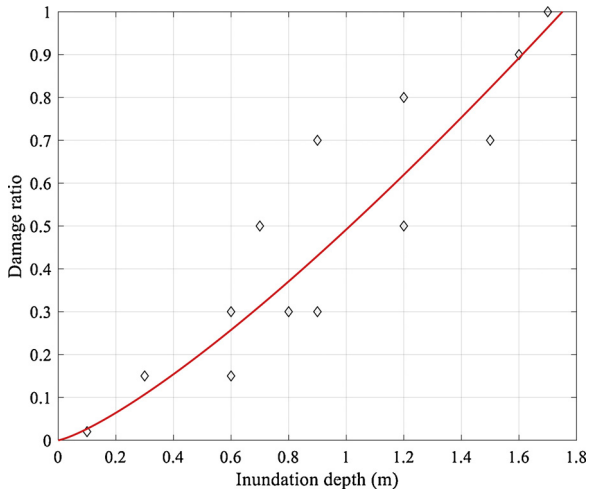

Fig. 6. Vulnerability function (depth-damage curve) for wattle and daub houses.

amongst low-income to poor people who could not afford modern and expensive housing. Similarly, wattle and daub is the most widely practiced in the slum areas and such areas generally occur in the river banks where land would be available free of cost. Thus, flood impact on wattle and daub buildings would be more pronounced not only due to their inherent vulnerabilities but also due to their vast presence in the flood-prone areas.

3.2.2. Flood vulnerability and fragility functions for wattle and daub dwellings

Based on the data collected during the field survey, we constructed a vulnerability curve for the wattle and daub construction system. The vulnerability curve considering the logit function was derived as shown in Fig. 6. As shown in Fig. 6, inundation up to 20 cm depicts the damage ratio less than 10 %, inundation of 50 cm leads to 20 % damage, inundation of 1 m leads to 50 % damage and inundation of 1.6 m results in 90 % damage to wattle and daub dwellings. Notably, slight to minor damages need scrutinized efforts to demarcate hence the lower inundation depths hardly contribute in construction of vulnerability curve, which is often regarded as the depth-damage curve. Obtaining discrete data points is challenging especially in the case of flood events because most of the heavily damaged and collapsed buildings would not show the actual impression of inundation depth. However, we assessed distinctly inundated and damage wattle and daub dwellings during the field survey. The inundation scenario comparable to the 2017 flood was reflected by the 20 years return period flood. The average inundation along the bank where the damage has occurred was ~1.5 m. Similarly, the average depth of inundation was also 1.5 m for the riverbank. This is evident that the 20 years return period can cause significant damage to wattle and daub buildings. Thus, to predict the probabilistic performance of wattle and daub constructions, vulnerability and fragility curves derived in this study play a vital role. Both vulnerability and fragility curves could be used to get the probability of damage/damage level exceedance for a particular inundation depth from any return period. At higher return periods, the inundation depth would be higher in general, the expected performance level or damage level of wattle and daub construction system could be estimated from Figs. 6 and 7.

We further processed the data to construct fragility functions for five damage classes. Among 34 damage cases, 12.5 % houses

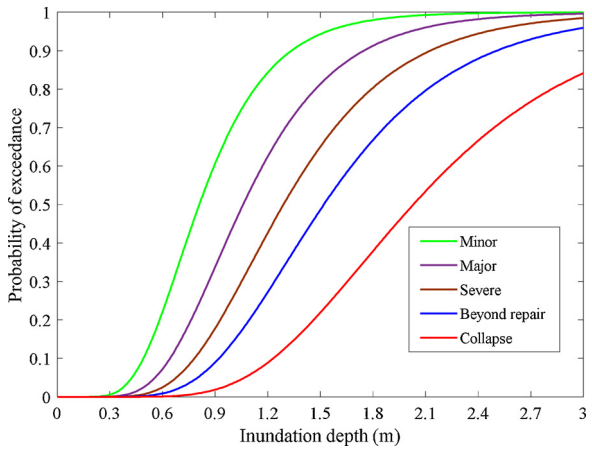

Fig. 7. Flood fragility functions for wattle and daub houses.

Table 1
Adjusted lognormal distribution parameters for wattle and daub houses.

Damage state (DS)	Lognormal distribution parameters	
	α (m)	β
Minor	0.81	0.39
Major	1.06	0.39
Severe	1.29	0.39
Beyond repair	1.52	0.39
Collapse	2.03	0.39

depicted minor damage, 25 % depicted major damage, 18.75 % depicted severe damage, 25 % depicted beyond repair damage, and 18.75 % depicted collapse damage state. Considering the mean damage ratio for each damage state, lognormal distribution parameters were estimated. However, the quality of fragility functions was not satisfactory due to the limited database that resulted in intersecting curves. Thereafter, we re-assessed the quality of fragility functions considering the distribution of standard deviation per Eqs. 4 and 5.

$$\beta_i^{'} = \frac{1}{N}\sum_{i=1}^{N}\beta_i \ldots \tag{4}$$

$$\alpha_i^{'} = e^{(1.28(\beta^{'}-\beta_i)+\ln\alpha_i)} \ldots \tag{5}$$

Herein, $\beta_i^{'}$ and $\alpha_i^{'}$ represent the adjusted lognormal standard deviation and median for particular damage state i. After distributing the lognormal standard deviations obtained initially, we adjusted the median parameter (α). The summary of corrected lognormal distribution parameters is presented in Table 1.

As all the preceding fragility curve intersected the following curve, the redistribution of the lognormal standard deviation resulted in the same value for all five classes. However, significant variation in terms of median depth of inundation (m) was observed as shown in Table 1. The parameters were then plotted to obtain the fragility functions for five damage states as shown in Fig. 7. Fig. 7 highlights that up to the inundation depth of 30 cm, only minor damages are expected. Similarly, initiation of collapse with the probability of exceedance less than 5% is expected after the inundation depth of 75 cm. At a depth of 1.2 m, the probabilities of exceedance of collapse, beyond repair, severe, major, and minor damage states are respectively 10 %, 25 %, 40 %, 70 %, and 90 %. As 1.2 m depth of inundation is quite common during every monsoon in the southern plains of Nepal, it could be concluded that most of the wattle and daub houses would not be usable at this depth. Thus, there is an urgent need for improvement in the wattle and daub housing construction system to assure flood resilience. As the total cost of construction of wattle and daub houses ranges between US$ 50–500, low-cost improvements are important because the owners cannot afford drastic improvements due to cost issues.

4. Conclusions

Flood hazard assessment is conducted for frequently flooding Khando River catchment in eastern Nepal. Using rainfall data of 47 years, we estimated inundation depths for the catchment and prepared flood hazard maps for 20, 50, 100, and 200 years return period. The results highlight that the maximum inundation depth does not vary significantly as highlighted by the range of 3.85–4.20 m for 20 and 200 years return periods respectively. More than 95 % of the study area is likely to observe inundation depth up to 1.5 m for all return periods considered in this study. The outcomes of the flood hazard assessment are subject to flood vulnerability analysis of existing building types using the survey data. Forensic interpretations of the damaged structures are reported in this study. We used the damage ratio and inundation depth to create vulnerability and fragility functions. The vulnerability analysis of the wattle and daub construction concludes that the wattle and daub houses would observe damage even at low inundation depth (up to 0.5 m). Meanwhile, at a depth of 1.7 m, most of the wattle and daub houses are expected to collapse. Fragility functions considering five damage grades are constructed in this study. The flood hazard maps indicate that 1.5 m inundation would commonly occur, hence, it is obvious that the wattle and daub construction system would be frequently affected by the flood causing enormous losses of lives and properties. The average measured inundation depth was nearly equal to the estimated inundation depth for 20 years return period flood, which highlights that the 2017 event was equivalent to 20 years return period rainfall. Even at the inundation depth of 1.7 m, more than 95 % of the wattle and daub houses would collapse as reflected by the newly developed fragility functions. Similarly, at a depth of inundation of 2.5 m, even poorly engineered RC buildings would collapse. The low rate of collapse and severe damage statistics is also attributed to a smaller number of buildings across the catchment. All the hazard maps depict that more than 95 % of areas would have inundation depth within 1.5 m. This indicates that the settlements with predominant wattle and daub constructions across the riverbanks would be severely affected by floods of low return periods too. The juxtaposition of fragility functions and flood hazard maps highlights that the wattle and daub constructions are highly vulnerable to even 20 years return period flood. For the non-perennial spring rivers, flood events are quite frequent, and loss of lives and properties is reported almost every year, thus, improvement of conventional wattle and daub system is urgent to save lives and properties in similar catchments. The fragility functions developed in this study represent the wattle and daub constructions in the southern plains of Nepal and may not represent the probability of damage occurrence for other environments such as the mountain torrents. Future studies may

incorporate calibration of discharge estimation method with recorded discharge data to obtain more representative discharge values. This may improve the flood mapping results in data-scarce environments such as the Khando River catchment. Similarly, the vulnerability and fragility functions may be also improved using more damage data. Coverage of broad areas during survey would also improve the quality of fragility functions as a more discrete database would be available.

CRediT authorship contribution statement

Saraswati Thapa: Conceptualization, Data curation, Formal analysis, Methodology, Software, Visualization, Writing - original draft, Writing - review & editing. **Anup Shrestha:** Data curation, Formal analysis, Software, Methodology, Writing - review & editing. **Suraj Lamichhane:** Conceptualization, Methodology, Visualization, Writing - review & editing. **Rabindra Adhikari:** Funding acquisition, Investigation, Methodology, Visualization, Writing - review & editing. **Dipendra Gautam:** Conceptualization, Data curation, Formal analysis, Funding acquisition, Investigation, Methodology, Visualization, Writing - original draft, Writing - review & editing.

Declaration of Competing Interest

Authors declare no conflict of interest in any form.

Acknowledgements

The authors acknowledge the travel support provided by Cosmos College of Management and Technology and Digicon Engineering Consult after the 2017 flood in eastern Nepal. The topographical survey data were generously provided by Bishnu Dev Yadav (Department of Irrigation, Government of Nepal), we express sincere thanks to him. The hydro-meteorological data used in this study was provided by Department of Hydrology and Meteorology, Government of Nepal. Discussions from Prem Chandra Jha were fruitful in selecting flood estimation methods. So, we are thankful to him. Authors express sincere thanks to Pratyush Jha, Bikalpa Aryal, Kamal Ghalan, Shristi Maharjan, Mamata Sayami, and Himal Tamang for their support. The constructive and meticulous comments from four anonymous reviewers and the editor-in-chief have improved the quality of the manuscript appreciably, so, they are acknowledged for their efforts.

References

Adhikari, R., Gautam, D., Jha, P., Aryal, B., Ghalan, K., Rupakhety, R., Dong, Y., Rodrigues, H., Motra, G., 2019. Bridging multi-hazard vulnerability and sustainability: approaches and applications to Nepali Highway Bridges. Resilient Structures and Infrastructure 361–378. https://doi.org/10.1007/978-981-13-7446-3_14.

Azmeri, A., Isa, A.H., 2018. An analysis of physical vulnerability to flash floods in the small mountainous watershed of Aceh Besar Regency, Aceh province, Indonesia. Jamba J. Disaster Risk Stud. 10 (1), 550.

Baradaranshoraka, M., Pinelli, J.P., Gurley, K., Zhao, M., Peng, X., Paleo-Torres, A., 2019. Characterization of coastal flood damage states for residential buildings. ASCE-ASME J. Risk Uncertain. Eng. Syst. Part A Civ. Eng. 5 (1). https://doi.org/10.1061/AJRUA6.0001006.

Ben Khalfallah, C., Saidi, S., 2018. Spatiotemporal floodplain mapping and prediction using HEC-RAS - GIS tools: case of the Mejerda river, Tunisia. J. Afr. Earth Sci. 142, 44–51.

Bourenane, H., Bouhadad, Y., Guettouche, M.S., 2019. Flood hazard mapping in urban area using the hydrogeomorphological approach: case study of the Boumerzoug and Rhumel alluvial plains (Constantine city, NE Algeria). J. Afr. Earth Sci. 160, 103602.

Cao, C., Xu, P., Wang, Y., Chen, J., Zheng, L., Niu, C., 2016. Flash flood hazard susceptibility mapping using frequency ratio and statistical index methods in coalmine subsidence areas. Sustain 8 (9), 948.

Central Bureau of Statistics Nepal, 2012. National Population and Housing Census 2011. Kathmandu. .

"Department of Hydrology and Meteorology." [Online]. Available: https://www.dhm.gov.np/.

De Risi, R., Jalayer, F., De Paola, F., Carozza, S., Yonas, N., Giugni, M., Gasparini, P., 2019. From flood risk mapping toward reducing vulnerability: the case of Addis Ababa. Nat. Hazards 100, 387–415.

Di Salvo, C., Pennica, F., Ciotoli, G., Cavinato, G.P., 2018. A GIS-based procedure for preliminary mapping of pluvial flood risk at metropolitan scale. Environ. Model. Softw. 107, 64–84.

ESRI, "Arc GIS." [Online]. Available: https://www.esri.com/en-us/arcgis/about-arcgis/overview.

Ezz, H., 2018. Integrating GIS and HEC-RAS to model Assiut plateau runoff. Egypt. J. Remote Sens. Sp. Sci. 21 (3), 219–227.

Fuchs, S., Heiser, M., Schlögl, M., Zischg, A., Papathoma-Köhle, M., Keiler, M., 2019a. Short communication: a model to predict flood loss in mountain areas. Environ. Model. Softw. 117, 176–180.

Fuchs, S., Heiss, K., Hübl, J., 2007. Towards an empirical vulnerability function for use in debris flow risk assessment. Nat. Hazards Earth Syst. Sci. Discuss. 7, 495–506.

Fuchs, S., Keiler, M., Ortlepp, R., Schinke, R., Papathoma-Köhle, M., 2019b. Recent advances in vulnerability assessment for the built environment exposed to torrential hazards: challenges and the way forward. J. Hydrol. 575, 587–595.

Gautam, D., 2017a. Assessment of social vulnerability to natural hazards in Nepal. Nat. Hazards Earth Syst. Sci. 17 (12), 2313–2320.

Gautam, D., 2017b. On seismic vulnerability of highway bridges in Nepal: 1988 Udaypur earthquake (M W 6.8) revisited. Soil Dyn. Earthq. Eng. 99 (August), 168–171.

Gautam, D., Dong, Y., 2018. Multi-hazard vulnerability of structures and lifelines due to the 2015 Gorkha earthquake and 2017 central Nepal flash flood. J. Build. Eng. 17, 196–201.

Gautam, D.K., Dulal, K., 2013. Determination of threshold runoff for flood warning in nepalese rivers. J. Integr. Disaster Risk Manag. 3 (1), 126–136.

Gautam, D., Prajapati, J., Paterno, K.V., Bhetwal, K.K., Neupane, P., 2016. Disaster resilient vernacular housing technology in Nepal. Geoenvironmental Disasters 3 (December (1)), 1–14.

Gautam, D., Fabbrocino, G., Santucci de Magistris, F., 2018. Derive empirical fragility functions for Nepali residential buildings. Eng. Struct. 171, 617–628.

Godfrey, A., Ciurean, R.L., van Westen, C.J., Kingma, N.C., Glade, T., 2015. Assessing vulnerability of buildings to hydro-meteorological hazards using an expert based approach - an application in Nehoiu Valley, Romania. Int. J. Disaster Risk Reduct. 13, 229–241.

Government of Nepal, 2009. Nepal Disaster Report 2009. Kathmandu. .

Government of Nepal, 2017. Nepal Flood 2017: Post Flood Recovery Needs Assessment. Kathmandu. .

Government of Nepal, "DRR Portal Nepal." [Online]. Available: http://www.drrportal.gov.np/.
Grimaldi, S., Petroselli, A., Arcangeletti, E., Nardi, F., 2013. Flood mapping in ungauged basins using fully continuous hydrologic-hydraulic modeling. J. Hydrol. (Amst) 487, 39–47.
Guzzetti, F., Stark, C.P., Salvati, P., 2005. Evaluation of flood and landslide risk to the population of Italy. Environ. Manage. 36, 15–36.
Hagen, E., Shroder, J.F., Lu, X.X., Teufert, J.F., 2010. Reverse engineered flood hazard mapping in Afghanistan: a parsimonious flood map model for developing countries. Quat. Int. 126 (1–2), 82–91.
Kang, H., Kim, Y., 2016. The physical vulnerability of different types of building structure to debris flow events. Nat. Hazards 80, 1475–1493.
Karagiorgos, K., Thaler, T., Hübl, J., Maris, F., Fuchs, S., 2016. Multi-vulnerability analysis for flash flood risk management. Nat. Hazards 82, 63–87.
Karki, R., ul Hasson, S., Schickhoff, U., Scholten, T., Böhner, J., 2017. Rising precipitation extremes across Nepal. Climate 5 (1), 4.
Kazakis, N., Kougias, I., Patsialis, T., 2015. Assessment of flood hazard areas at a regional scale using an index-based approach and Analytical Hierarchy process: application in Rhodope-Evros region, Greece. Sci. Total Environ. 538, 555–563.
Khanal, N.R., Shrestha, M., Ghimire, M., 2007. Preparing for Flood Disaster: Mapping and Assessing Hazard in the Ratu Watershed, Nepal. Kathmandu. .
Lamichhane, S., Shakya, N.M., 2019a. Alteration of groundwater recharge areas due to land use/cover change in Kathmandu Valley, Nepal. J. Hydrol. Reg. Stud. 26, 100635.
Lamichhane, S., Shakya, N.M., 2019b. Integrated assessment of climate change and land use change impacts on hydrology in the Kathmandu Valley watershed, Central Nepal. Water (Switzerland) 11 (10), 2059.
Maidment, D.R., 1992. Handbook of Hydrology. McGraw-Hill Education.
Marchi, L., Borga, M., Preciso, E., Gaume, E., 2010. Characterisation of selected extreme flash floods in Europe and implications for flood risk management. J. Hydrol. 394 (1–2), 118–133.
Miranda, F.N., Ferreira, T.M., 2019. A simplified approach for flood vulnerability assessment of historic sites. Nat. Hazards 96, 713–730.
Mishra, B.K., Herath, S., 2015. Assessment of future floods in the Bagmati River Basin of Nepal using bias-corrected daily GCM precipitation data. J. Hydrol. Eng. 20 (8). https://doi.org/10.1061/(ASCE)HE.1943-5584.0001090.
Nharo, T., Makurira, H., Gumindoga, W., 2019. Mapping floods in the middle Zambezi Basin using earth observation and hydrological modeling techniques. Phys. Chem. Earth 114, 102787.
NPC, 2017. Post Flood Recovery Need Assessment. Kathmandu. .
Ntajal, J., Lamptey, B.L., Mahamadou, I.B., Nyarko, B.K., 2017. Flood disaster risk mapping in the Lower Mono River Basin in Togo, West Africa. Int. J. Disaster Risk Reduct. 23, 93–103.
Papathoma-Köhle, M., Keiler, M., Totschnig, R., Glade, T., 2012. Improvement of vulnerability curves using data from extreme events: debris flow event in South Tyrol. Nat. Hazards 64, 2083–2105.
Parisi, F., Sabella, G., 2017. Flow-type landslide fragility of reinforced concrete framed buildings. Eng. Struct. 131, 28–43.
Pavlova, A.I., 2017. Analysis of elevation interpolation methods for creating digital elevation models. Optoelectron. Instrum. Data Process. 53, 171–177.
Popa, M.C., Peptenatu, D., Draghici, C.C., Diaconu, D.C., 2019. Flood hazard mapping using the flood and Flash-Flood Potential Index in the Buzau River catchment, Romania. Water (Switzerland) 11 (10), 2116.
Porter, K., Kennedy, R., Bachman, R., 2007. Creating fragility functions for performance-based earthquake engineering. Earthq. Spectra 23 (2), 471–489.
Quan Luna, B., Blahut, J., Van Westen, C.J., Sterlacchini, S., Van Asch, T.W.J., Akbas, S.O., 2011. The application of numerical debris flow modelling for the generation of physical vulnerability curves. Nat. Hazards Earth Syst. Sci. 11, 2047–2060.
Rossetto, T., Elnashai, A., 2005. A new analytical procedure for the derivation of displacement-based vulnerability curves for populations of RC structures. Eng. Struct. 27 (February (3)), 397–409.
Santo, A., Santangelo, N., Forte, G., De Falco, M., 2016. Post flash flood survey: the 14th and 15th October 2015 event in the Paupisi-Solopaca area (Southern Italy). J. Maps 13 (2), 19–25.
Santos, M., Santos, J.A., Fragoso, M., 2015. Historical damaging flood records for 1871-2011 in Northern Portugal and underlying atmospheric forcings. J. Hydrol. 530, 591–603.
Sarhadi, A., Soltani, S., Modarres, R., 2012. Probabilistic flood inundation mapping of ungauged rivers: linking GIS techniques and frequency analysis. J. Hydrol. 458–459, 68–86.
Shadmehri Toosi, A., Calbimonte, G.H., Nouri, H., Alaghmand, S., 2019. River basin-scale flood hazard assessment using a modified multi-criteria decision analysis approach: a case study. J. Hydrol. 574, 660–671.
Shinozuka, M., Feng, M.Q., Lee, J., Naganuma, T., 2002. Statistical analysis of fragility curves. J. Eng. Mech. 126 (12). https://doi.org/10.1061/(ASCE)0733-9399(2000)126:12(1224).
"SRTM Digital Elevation Database." [Online]. Available: http://srtm.csi.cgiar.org/.
Talchabhadel, R., Karki, R., Thapa, B.R., Maharjan, M., Parajuli, B., 2018. Spatio-temporal variability of extreme precipitation in Nepal. Int. J. Climatol. 38 (11), 4296–4313.
Totschnig, R., Fuchs, S., 2013. Mountain torrents: quantifying vulnerability and assessing uncertainties. Eng. Geol. 155, 31–44.
Tsakiris, G., 2014. Flood risk assessment: concepts, modelling, applications. Nat. Hazards Earth Syst. Sci. 14, 1361–1369.
US Army Corps of Engineers, "HEC-RAS." [Online]. Available: https://www.hec.usace.army.mil/software/hec-ras/.
Zhang, D., Quan, J., bin Zhang, H., Wang, F., Wang, H., yan He, X., 2015. Flash flood hazard mapping: a pilot case study in Xiapu River Basin, China. Water Sci. Eng. 8 (3), 195–204.
Zhao, G., Xu, Z., Pang, B., Tu, T., Xu, L., Du, L., 2019. An enhanced inundation method for urban flood hazard mapping at the large catchment scale. J. Hydrol. 571, 873–882.